

**The incorporation of an organic soil layer in the Noah-MP Land Surface Model and its
evaluation over a Boreal Aspen Forest**

Liang Chen^{1,2}, Yanping Li¹, Fei Chen³, Alan Barr⁴, Michael Barlage³, and Bingcheng Wan³

¹Global Institute for Water Security, University of Saskatchewan, Saskatoon, SK, Canada

²Key Laboratory of Regional Climate Environment for Temperate East Asia, Institute of Atmospheric Physics, Chinese Academy of Sciences, Beijing, China

³National Center for Atmospheric Research, Boulder, Colorado

⁴Environment Canada, National Hydrology Research Center, Saskatoon, SK, Canada

Corresponding author address:

Yanping Li

Global Institute for Water Security

School of Environment and Sustainability

University of Saskatchewan

Phone: 306-966-2793

E-mail: yanping.li@usask.ca

Abstract

A thick top layer of organic matter is a dominant feature in boreal forests and can impact land-atmosphere interactions. In this study, the multi-parameterization version of the Noah land-surface model (Noah-MP) was used to investigate the impact of incorporating a forest-floor organic soil layer on the simulated surface energy and water cycle components at the BERMS Old Aspen Flux (OAS) field station in central Saskatchewan, Canada. Compared to a simulation without an organic soil parameterization (CTL), the Noah-MP simulation with an organic soil (OGN) improved Noah-MP simulated soil temperature profiles and soil moisture at 40-100cm, especially the phase and amplitude (Seasonal cycle) of soil temperature below 10 cm. OGN also enhanced the simulation of sensible and latent heat fluxes in spring, especially in wet years, which is mostly related to the timing of spring soil thaw and warming. Simulated top-layer soil moisture is better in OGN than that in CTL in summer but worse in winter. The effects of including an organic soil layer on soil temperature are not uniform throughout the soil depth and are more prominent in summer. For drought years, the OGN simulation substantially modified the partitioning of water between direct soil evaporation and vegetation transpiration. For wet years, the OGN simulated latent heat fluxes are similar to CTL except for spring season where OGN produced less evaporation, which was closer to observations. Including organic soil produced more sub-surface runoff and resulted in much higher runoff throughout the season in wet years.

Keywords Organic soil, Noah-MP, surface energy and water budgets, BERMS

1 **1. Introduction**

2 Land surface processes play an important role in the climate system by controlling land-
3 atmosphere exchanges of momentum, energy and mass (water, carbon dioxide, and aerosols).
4 Therefore, it is critical to correctly represent these processes in land surface models (LSMs) that
5 are used in weather prediction and climate models (e.g., Dickinson et al. 1986; Sellers et al. 1996;
6 Chen and Dudhia 2001; Dai et al. 2003; Oleson et al. 2008, Niu et al. 2011). Niu et al. (2011) and
7 Yang et al. (2011) developed the Noah LSM with multi-parameterization options (Noah-MP) and
8 evaluated its simulated seasonal and annual cycles of snow, hydrology, and vegetation in different
9 regions. Noah-MP has been implemented in the community Weather Research and Forecasting
10 (WRF) model (Barlage et al. 2015), which is widely used as a numerical weather prediction and
11 regional climate model for dynamical downscaling in many regions world-wide (Chotamonsak et
12 al., 2012). The performance of Noah-MP was previously evaluated using in-situ and satellite data
13 (Niu et al. 2011, Yang et al. 2011, Cai et al. 2014, Pilotto et al. 2015, Chen et al. 2014). Those
14 evaluation results showed significant improvements in modeling runoff, snow, surface heat fluxes,
15 soil moisture, and land skin temperature compared to the Noah LSM (Chen et al. 1996, Ek et al.
16 2003). Recently, Chen et al. (2014) compared Noah-MP to Noah and four other LSMs regarding
17 the simulation of snow and surface heat fluxes at a forested site in the Colorado Headwaters region,
18 and found a generally good performance of Noah-MP. However, it is challenging to parameterize
19 the cascading effects of snow albedo and below-canopy turbulence and radiation transfer in
20 forested regions as pointed out by Clark et al. (2015) and Zheng et al. (2015).

21 The Canadian boreal region contains one third of the world's boreal forest, approximately
22 6 million km² (Bryant et al. 1997). The boreal forests have complex interactions with the
23 atmosphere and have significant impacts on regional and global climate (Bonan, 1991; Bonan et

24 al., 1992; Thomas and Rowntree, 1992; Viterbo and Betts, 1999; Ciais et al., 1995). Several field
25 experiments were conducted to better understand and model these interactions, including
26 BOREAS (Boreal Ecosystem Atmosphere Study) and BERMS (Boreal Ecosystem Research and
27 Monitoring Sites). Numerous studies have evaluated LSMs using the BOREAS and BERMS data
28 (Bonan et al. 1997). Levine and Knox (1997) developed a frozen soil temperature (FroST) model
29 to simulate soil moisture and heat flux and used BOREAS northern and southern study areas to
30 calibrate the model. They found that soil temperature was underestimated and large model biases
31 existed when snow was present. Bonan et al. (1997) examined NCAR LSM1 with flux-tower
32 measurements from the BOREAS, and found that the model reasonably simulated the diurnal cycle
33 of the fluxes. Bartlett et al. (2002) used the BOREAS Old Jack Pine (OJP) site to assess two
34 different versions of CLASS, the Canadian Land Scheme (2.7 and 3.0) and found that both versions
35 underestimated the snow depth and soil temperature values, especially the version CLASS 2.7.

36 Boreal forest soils often have a relatively thick upper organic horizon. The thickness of the
37 organic horizon directly affects the soil thermal regime and indirectly affects soil hydrological
38 processes. Compared with mineral soil, the thermal and hydraulic properties of the organic soil are
39 significantly different. Dingman (1994) found that the mineral soil porosity ranges from 0.4 to 0.6,
40 while the porosity of organic soil is seldom less than 0.8 (Radforth et al., 1977). The hydraulic
41 conductivity of organic soil horizons can be very high due to the high porosity (Boelter, 1968).
42 Less suction is observed for given volumetric water content in organic soils than in mineral soils
43 except when it reaches saturation. The thermal properties of the soil are also affected by the
44 underground hydrology. Organic soil horizons also have relatively low thermal conductivity,
45 relatively high heat capacity and a relatively high fraction of plant-available water. Prior studies
46 illustrated the importance of parameterizing organic soil horizons in LSMs for simulating soil

47 temperature and moisture (e.g., Letts et al. 2000, Beringer et al. 2001, Molders and Romanovsky
48 2006, Nicolsky et al. 2007, Lawrence and Slater 2008).

49 The current Noah-MP model does not include a parameterization for organic soil horizons.
50 It is thus critical to evaluate the effects of incorporating organic matter on surface energy and water
51 budgets in order to enhance the global applicability of the WRF-Noah-MP coupled modeling
52 system. Here we conduct a detailed examination of the performance of the Noah-MP model in a
53 Canadian boreal forest site. The main objective of this research is to enhance the modeling of
54 vertical heterogeneity (such as organic matter) in soil structures and to understand its impacts on
55 the simulated seasonal and annual cycle of soil moisture and surface heat fluxes. We recognize
56 that Noah-MP has weaknesses in existing sub-process parameterizations, while the goal of this
57 study is to explore the impact of incorporating organic soil on surface energy and water budgets,
58 rather than comprehensively addressing errors in existing Noah-MP parameterization schemes. In
59 this paper, we present the BERMS observation site in central Saskatchewan (Section 2), and our
60 methodology for conducting 12-year Noah-MP simulations with and without organic soil layer for
61 that boreal forest site (Section 3). Section 4 discusses the simulations of the diurnal and annual
62 cycles of the surface energy and hydrological components, in dry and wet periods. Summary and
63 conclusions are given in Section 5.

64

65 **2. BERMS site descriptions**

66 The Old Aspen Site (OAS, 53.7°N, 106.2°W, altitude 601 m) is located in mature
67 deciduous broadleaf forest at the southern edge of the Canadian boreal forest in Prince Albert
68 National Park, Saskatchewan, Canada (Figure 1). The forest canopy consists of a 22-m trembling
69 aspen overstory (*Populus tremuloides*) with ~10% balsam poplar (*Populus balsamifera*.) and a 2-

70 m hazelnut understory (*Corylus cornuta*) with sparse alder (*Alnus crispa*). The fully-leafed values
71 of the leaf area index varied among years from 2.0 to 2.9 for the aspen overstory and 1.5 to 2.8 for
72 the hazelnut understory (Barr et al. 2004). The forest was regenerated after a natural fire in 1919,
73 and in 1998 it had a stand density of ~830 stems ha⁻¹. The soil is an Orthic Gray Luvisol (Canadian
74 Soil Classification System) with an 8-10 cm deep forest-floor (LFH) organic horizon overlying a
75 loam Ae horizon (0-21 cm), a sandy clay loam Bt horizon (21-69 cm), and a sandy clay loam Ck
76 horizon (69+ cm) . 30% of the fine roots are in the LFH horizon and 60% are in the upper 20 cm
77 of mineral soil. The water table lies from 1 to 5 m below the ground surface, varying spatially in
78 the hummocky terrain and varying in time in response to variations in precipitation. A small
79 depression near the tower had ponded water at the surface during the wet period from 2005 to 2010.
80 Mean annual air temperature and precipitation at the nearest long-term weather station are 0.4 °C
81 and 467 mm, respectively (Waskesiu Lake, 53°55'N, 106°04'W, altitude 532 m, 1971-2000
82 climatic normal).

83 Air temperature and humidity were measured at 36-m above ground level using a Vaisala
84 model HMP35cf or HMP45cf temperature/humidity sensor (Vaisala Oyj, Helsinki, Finland) in a
85 12-plate Gill radiation shield (R.M. Young model 41002-2, Traverse City, MI, USA). Windspeed
86 was measured using a propeller anemometer (R.M. Young model 01503-, Traverse City, MI, USA)
87 located at 38-m above ground level. Atmospheric pressure was measured using a barometer (Setra
88 model SBP270, distributed by Campbell Scientific Inc., Logan, UT, USA). Soil temperature was
89 measured using thermocouples in two profiles at depths of 2, 5, 10, 20, 50 and 100 cm. The two
90 upper measurements were in the forest-floor LFH. Soil volumetric water content was measured
91 using TDR probes (Moisture Point Type B, Gabel Corp., Victoria, Canada) with measurements at
92 depths of 0-15, 15-30, 30-60, 60-90 and 90-120 cm. Three of the eight probes that were the most

93 free of data gaps were used in this analysis. The TDR probes were located in a low-lying area of
94 the site that was partially flooded after 2004, resulting in high Volumetric Water Content (VWC)
95 values that may not be characteristic of the flux footprint. VWC is also measured at 2.5- and 7.5-
96 cm depth in the forest-floor LFH layer using two profiles of soil moisture reflect meters (model
97 CS615, Campbell Scientific Inc., Logan, UT, USA), inserted horizontally at a location that did not
98 flood.

99 Eddy-covariance measurements of the sensible and latent heat flux densities were made at
100 39 m above the ground from a twin scaffold tower. Details of the eddy-covariance systems are
101 given in Barr et al. (2006). Data gaps were filled using a standard procedure (Amiro et al. 2006).

102 The net radiation flux density, R_n , was calculated from component measurements of
103 incoming and outgoing shortwave and longwave radiation, made using paired Kipp and Zonen
104 (Delft, The Netherlands) model CM11 pyranometers and paired Eppley Laboratory (Newport, RI,
105 USA) model PIR pyrgeometers. The upward-facing radiometers were mounted atop the scaffold
106 flux tower in ventilated housings to minimize dew and frost on the sensor domes. The net
107 radiometer and the downward-facing radiometers were mounted on a horizontal boom that
108 extended 4 m to the south of the flux tower, ~ 10 m above the forest canopy. Details of the minor
109 terms in the surface energy balance; including soil heat flux and biomass heat storage flux are
110 given in Barr et al. (2006). During the warm season when all components of the surface energy
111 balance were resolved, the sum of the eddy-covariance sensible and latent heat fluxes
112 underestimated the surface available energy (net radiation minus surface storage) by ~15% (Barr
113 et al. 2006).

114

115 **3. Methodology**

116 3.1 *The Noah-MP Land-Surface Model*

117 Noah-MP is a new-generation of LSM, which was developed to improve the performance
118 of the Noah LSM (Chen et al. 1996; Chen and Dudhia 2001). It is coupled to the WRF community
119 weather and regional climate model (Barlage et al. 2015), and also available as a stand-alone 1-D
120 model (Noah-MP v1.1). Noah-MP simulates several biophysical and hydrological processes that
121 control fluxes between the surface and the atmosphere. These processes include surface energy
122 exchange, radiation interactions with the vegetation canopy and the soil, hydrological processes
123 within the canopy and the soil, a multi-layer snowpack with freeze-thaw, groundwater dynamics,
124 stomatal conductance, and photosynthesis and ecosystem respiration. The major components
125 include a 1-layer canopy, 3-layer snow, and 4-layer soil. Noah-MP provides a multi-
126 parameterization framework that allows using the model with different combinations of alternative
127 process schemes for individual processes (Niu et al., 2011). Alternative sub-modules for 12
128 physical processes can provide more than 5000 different combinations. Soil water fluxes are
129 calculated by the Richards equation using a Campbell/Clapp-Hornberger parameterization of the
130 hydraulic functions (Clapp and Hornberger, 1978).

131 We use an off-line stand-alone 1-D mode (Noah-MP) with four soil layers: 0-10cm, 10-
132 40cm, 40-100cm, and 100-200 cm. The selected Noah-MP physics options used in this study are
133 similar to Barlage et al. (2015), Gao et al. (2015) and Chen et al. (2014) and are list in Table 1. In
134 the default configuration of Noah-MP, the entire vertical soil profile was treated as one mineral
135 ground texture only, and no organic soil matter is included.

136 The OAS research site has an organic LFH (forest-floor) soil horizon, 8~10 cm deep. This
137 study evaluates the impact of adding an organic soil horizon in the Noah-MP model using a similar
138 approach to Lawrence and Slater (2008), which parameterizes soil thermal and hydrologic

139 properties in terms of carbon density in each soil layer. Soil carbon or organic fraction for each
140 layer is determined as

$$141 \quad f_{sc,i} = \frac{\rho_{sc,i}}{\rho_{sc,max}} \quad (1)$$

142 where $f_{sc,i}$ is the carbon fraction of the each layer, $\rho_{sc,i}$ is the soil carbon density, and $\rho_{sc,max}$ is
143 the maximum possible value (peat density of 130 kg m⁻³, Farouki 1981). The soil properties for
144 each layer are specified as a weighted combination of organic and mineral soil properties.

$$145 \quad P = (1 - f_{sc,i})P_m + f P_o \quad (2)$$

146 where P_m is the value for mineral soil, P_o is the value for organic soil, and P is the weighted
147 average quantity. In this study, we assume that the top layer of the soil is made up of 100% organic
148 matter, consistent with the 8-10 cm LFH horizon at OAS. The remaining soil layers were assumed
149 that made up of 100% mineral soil. To investigate impacts of uncertainties of those parameters on
150 simulations, we conducted sensitive tests for key parameters such as saturated hydraulic
151 conductivity, porosity, suction, and Clapp and Hornberger parameter. Those parameters were
152 perturbed within a 5-20% range (except for hydraulic conductivity that is changed over 4 times
153 below and above the default value) following the work of Letts et al. (2000). Results showed that
154 the simulated soil moisture is not sensitive to these parameters perturbations, and the simulated
155 soil moisture and temperature results are not sensitive to the changes in porosity, saturated suction,
156 and hydraulic conductivity. This implies that the model results are not as sensitive to specific soil
157 parameter uncertainty as they are to differences in physical properties between CTL and OGN.
158 Therefore, we decided to use literatures (Lawrence and Slater, 2008, Letts et al., 2000)
159 recommended values instead, which produced soil moisture and soil temperature close to
160 observations (see Table 2).

161 *3.2 Forcing data*

162 The 30-min meteorological observations, including air temperature, specific humidity,
163 wind speed, pressure, precipitation, downward solar, and longwave radiation, at 36-m height from
164 OAS were used as atmospheric forcing data to drive Noah-MP in an off-line 1-D mode. Figure 2
165 shows the annual mean temperature (1.5 °C) and total precipitation (406 mm) at this site during
166 the study period (1998-2009). The most significant climatic features during the study period are a
167 prolonged drought that began in July 2001 and extended throughout 2003, and an extended wet
168 period from 2004-2007.

169

170 *3.3 Evaluation of model performance*

171 Outputs from the Noah-MP simulations were evaluated against observations, using the
172 Root Mean Squared Error (RMSE), square of the correlation coefficient (R^2), and Index of
173 Agreement (IOA) (Zhang et al. 2013). The IOA is calculated as

174
$$IOA = 1 - \frac{\sum_{i=1}^N (M_i - O_i)^2}{\sum_{i=1}^N (|O_i - \bar{O}| + |M_i - \bar{O}|)^2} \quad (3)$$

175 Where M_i and O_i are simulated and observed values of the same variable, respectively, and \bar{O}
176 is the mean of the observed values. *IOA* ranges from 0 (no agreement) to 1 (perfect match).

177

178 **4. Results and Discussions**

179 *4.1 Noah-MP model Spin-up*

180 The LSM spin-up is broadly defined as an adjustment processes as the model approaches
181 its equilibrium following the initial anomalies in soil moisture content or after some abnormal

182 environmental forcing (Yang et al., 1995). Without spin-up, the model results can be unstable and
183 may exhibit drift as model states try to approach their equilibrium values. To initialize LSMs
184 properly, the spin-up time required for LSMs to reach the equilibrium stage needs to be examined
185 first (Chen and Mitchell 1999, Cosgrove et al. 2003). In this study, model runs for the year 1998
186 were performed repeatedly until all the soil-state variables reached the equilibrium state, defined
187 as when the difference between two consecutive one-year simulations becomes less than 0.1% for
188 the annual means (Cai et al., 2014; Yang et al., 1995). Yang et al. (1995) discussed the spin-up
189 processes by comparing results from 22 LSMs for grass and forest sites, and showed a wide range
190 of spin-up timescales (from 1 year to 20 years), depending on the model, state variable and
191 vegetation type. Cosgrove et al. (2003) used four NLDAS-1 LSMs to discuss the spin-up time at
192 selected six sub-regions covering North America, and showed that all models reached equilibrium
193 between one to three years for all six sub-regions. In this study, we found that it requires 9 years
194 for deep-soil moisture (100-200 cm layer) in Noah-MP to reach its equilibrium, 8 years for latent
195 heat flux and evapotranspiration, but only 3 years for the surface soil moisture (Figure 3). Cosgrove
196 et al. (2003) and Chen et al. (1999) indicated that it takes long time to reach equilibrium especially
197 in the deep soil layers and sparse vegetation because the evaporation was limited by slow water
198 diffusion time scales between the surface and deep soil layers. When using the groundwater
199 component of Noah-MP, it might take at least 250 years to spin-up the water table depth in arid
200 regions (Niu et al., 2007). Cai et al. (2014) found that water table depth requires less than 10 years
201 to spin-up in a wet region, but more than 72 years for a dry region. For this boreal forest site where
202 the water table depth is shallower (less than 2.5 m), it takes ~7 years for water table depth to reach
203 equilibrium. However, the freezing/thawing is a relatively slow process, so we set 10 years for the
204 spin-up time for all the experiments discussed here.

205

206 *4.2 Seasonal cycle of soil temperature and moisture*

207 We defined the simulation without incorporating organic soil as the “control experiment”
208 (CTL); the simulation with the organic soil incorporated as the “organic layer experiment” (OGN).
209 We first evaluated the simulated CTL soil temperature and moisture at the OAS site in relation to
210 observations for the period of 1998-2009.

211 As shown in Figure 4, the effects of including an organic soil layer at the top (0~10cm) on
212 simulated soil temperature are not uniform both throughout the soil depth and during the year.
213 Figure 4a shows the CTL and OGN simulations produced nearly identical top-layer temperature
214 and are in agreement with the observations except for a low bias in the winter period, especially
215 during drought years 2002-2003. However, for deep layers (10-100cm), the OGN simulated much
216 lower (higher) soil temperatures during summer (winter), especially for the drought years 2002-
217 2003, leading to a good agreement between OGN and observations for 2nd and 3rd layer soil
218 temperature (Figure 4b, c). Lawrence and Slater (2008) indicated that strong cooling in summer is
219 due to the modulation of early and mid-summer soil heat flux, while higher soil temperature in fall
220 and winter is due to less efficient cooling of organic soils. The soil thawing period in spring is
221 significantly affected by the OGN parameterization since the thermal conductivity of the organic
222 horizon is much lower than that of the mineral soil ($\sim 0.4 \text{ W m}^{-1} \text{ K}^{-1}$ compared to $\sim 2.0 \text{ W m}^{-1} \text{ K}^{-1}$),
223 which delays the warming of the deep soil layers after snowmelt. In winter, the organic soil layer
224 insulates the soil and results in relatively higher wintertime soil temperatures for OGN compared
225 with CTL. The difference is most pronounced in drought years (2002 and 2003) (Figure 4) when
226 the thinner snowpack provides less insulation, leading to higher evaporation, which reduces soil
227 moisture. With an organic soil horizon, the OGN produces lower (higher) liquid soil water content

228 during winter (summer) in the topsoil layer (Figure 5). Lower (higher) soil moisture reduces
229 (increases) thermal heat conductivity, and results in higher (lower) winter (summer) soil
230 temperature in OGN as compared to CTL. These results are consistent with studies that showed a
231 simulated increase in winter soil temperature of up to 5 °C in boreal regions when including an
232 organic layer (Koven et al., 2009; Rinke et al., 2008; Lawrence and Slater, 2008) in LSMs.

233 For the top soil layer, the OGN parameterization increases the liquid soil water content in
234 summer as water fills the larger pore space of organic soil, but decreases the liquid soil water
235 content in winter, due to the contrasting water retention characteristics of organic and mineral soil
236 (Koven et al., 2009; Rinke et al., 2008; Lawrence and Slater, 2008). Higher porosity in OGN leads
237 to an increase in total soil water content, while lower the topsoil temperatures (Figure 4a) in OGN
238 with enhanced the ice content. Note that the observed soil water content during wet years may be
239 higher than the site truth because the sensors were located in a low spot that is prone to flooding.
240 This site got flooded in 2004 and the ground water has not dried since then, so that the soil was
241 oversaturated during the period of 2004-2008. In the second soil layer, the observed soil water
242 content was incorrect after the site got flooded (2004-2008). With more precipitation for this wet
243 period, the real soil water content should have a relatively high value. Since the OGN increases
244 the soil water content, it should be closer to the true observation. From figure 5, it can be seen that
245 the OGN improved the liquid water simulation in non-frozen periods. The soil moisture data are
246 not reliable when the soil is frozen and are therefore not very useful during the winter. In late
247 spring when snow starts melting, both CTL and OGN simulate the same topsoil temperature
248 (Figure 4). It is clear that the soil liquid water content is mainly controlled by precipitation, soil
249 hydraulic conductivity and runoff. The high porosity of organic soil in the topsoil layer helps to
250 retain more snowmelt water and hence increases the topsoil layer liquid water content. For the

251 deep soil layers, the soil liquid water content is highly influenced by the soil temperature. Liquid
252 soil water content increases during soil ice thawing period. The higher deep soil layer liquid water
253 content in OGN is mainly because the soil hydraulic conductivity is higher for organic soil than
254 mineral soil, so liquid water in the first-layer can be transported downward quickly into the deeper
255 layers. Although the organic soil layer is only added to the top layer in this study, it still can affect
256 the deep layer due to the infiltration characteristics of the topsoil.

257 The water retention characteristics of the organic soil horizon favor both higher water
258 retention and reduced evaporation. The thermal conductivity is lower compared with that of the
259 mineral soil, which then prevents the deeper soil to warm up rapidly after snowmelt season. The
260 lower thermal conductivity of the top organic soil affects the annual cycle of the ground heat flux.
261 In summer, the top layer is warmer than the deep layers, the ground heat flux then transfers heat
262 downward. Because air temperature is lower than land surface temperature so heat is transferred
263 upward from soil to the land surface, the lower thermal conductivity of the organic soil can prevent
264 the soil to cool. On the other hand, the snowfall in winter may form a snow layer that will insulate
265 the soil and make the simulations less sensitive to thermal conductivity. This may be the reason
266 why the OGN simulated soil temperature is increased in winter compared to CTL simulations.
267 With the organic soil layer on the top, the lower liquid soil water content in the topsoil layer during
268 winter time (Figure 5) reduces the heat loss through evaporation; the winter soil temperature then
269 becomes significantly higher compared with CTL experiment, while the higher soil water content
270 in the topsoil layer during summer time (Figure 5) increases the heat loss through evaporation; the
271 summer soil temperature then becomes significantly lower compared with CTL experiment.

272

273 *4.3 Seasonal cycles of sensible and latent heat flux*

274 Simulated differences in top-layer soil temperature and liquid soil water content lead to the
275 differences in simulated surface energy fluxes. Figure 6 show that the CTL run captures the
276 observed monthly mean sensible heat and latent heat flux reasonably well. However, SH is
277 underestimated in spring and overestimated in summer. Accordingly, LH is overestimated in
278 spring and underestimated in summer during most of the time period except for drought years
279 2002-2003 where LH is slightly overestimated. Generally, the OGN simulations show similar
280 characteristics to the CTL, with improved correlation coefficients between observations and
281 simulations: increasing from 0.81 (CTL) to 0.86 (OGN) for SH and from 0.94 (CTL) to 0.96 (OGN)
282 for LH (Figure 7). Overall, both CTL and OGN perform better in winter with snow cover, and the
283 differences between CTL and OGN is small. During the spring snow-melting season, the OGN
284 results are much better than the CTL (Figures 6 and 7).

285 The OGN simulations also improved the underestimation of SH in spring in CTL, but it
286 still overestimates summer SH. The reason for high bias in summer SH will be further discussed
287 in Section 4.4. SH and especially LH show improvement in OGN compared to CTL, which is
288 related to timing of soil thaw and warming in spring. CTL thaws the soil too early causing a
289 premature rise in LH in spring (April-May) and an associated underestimation of spring SH. The
290 spring (April-May) fluxes are much improved in the OGN parameterization. However, both OGN
291 and CTL retain a serious positive bias in SH from June-September, especially for wet years. The
292 reduction of surface layer saturation levels in OGN led to lower soil evaporation and associated
293 reductions in the total latent heat flux, and the reduction of LH is accompanied by a rise in SH
294 (Figure 6).

295

296 *4.4 Impact of organic soil on diurnal cycle of surface energy and hydrology*

297 The quality of nighttime flux-tower data is questionable (Chen et al. 2015), especially for
298 OAS located at boreal forest. Therefore, we focused our analysis on daytime observation data. In
299 general, the OGN parameterization improved the simulation of daily daytime LH in terms of both
300 RMSE and IOA, and increased IOA for SH (Table 3). Nevertheless, compared with CTL, OGN
301 increased the bias in SH slightly by ~6% (Table 3).

302 For the 12-year simulation period, the study site experienced a prolonged drought,
303 beginning in July 2001 and extended throughout 2002 and 2003. We choose year 2002 and 2003
304 to represent typical drought years, and year 2005 and 2006 to represent typical wet years (Figure
305 2), to examine the effect of the organic soil under different climate conditions. For drought years
306 (2002-2003), OGN increased daytime SH especially in spring, and slightly decreased SH at
307 nighttime (Figure 8a, b, c, and d). LH is well simulated by both OGN and CTL (Figure 8e, f, g,
308 and h), with OGN reducing daytime LH slightly. OGN overestimates daytime SH compared with
309 observations, while CTL underestimates daytime SH for spring (Figure 8a) and both OGN and
310 CTL slightly overestimates SH for summer, autumn and winter (Figure 8b, c, d). OGN has a major
311 impact on the daily cycle of soil temperature. Consistent with discussions in Section 4.2, the soil
312 temperature below 10 cm simulated by OGN is lower in summer and higher in winter than that of
313 the CTL simulation, and the OGN simulation has less bias than the CTL simulation (Figure 4). In
314 OGN simulation, the water moves faster into deep layers than in CTL simulation, leading to more
315 infiltrated water in the deep soil and hence higher base flow. Consequently, the total runoff is
316 increased. Due to the high soil porosity of the organic soil, OGN simulation shows higher soil-ice
317 fraction at the top soil layer during the freezing periods. The higher water capacity and higher soil-
318 ice fraction of the organic soil then reduce liquid water content/soil moisture, these further lead to

319 less evaporation (i.e., latent heat flux) during freezing periods (Spring), and a compensating
320 increase of the sensible heat flux.

321 For wet years (Figure 9), OGN produces in general higher daytime SH than CTL. For
322 spring, OGN simulated SH agrees with the observation better than CTL, but it is similar to or
323 slightly worse than CTL for other seasons. Simulated LH for both OGN and CTL agree with
324 observations well, with a significant improvement by OGN in spring. Note that the OGN
325 simulation also improves latent heat fluxes significantly in drought years, because the snowmelt
326 process dominates during spring months. For other seasons, the OGN results are fairly close to
327 CTL.

328 It is clear from Figures. 4, 8 and 9 that in both CTL and OGN, summer sensible heat fluxes
329 are overestimated for wet and dry years. We hypothesized that such high bias in summer sensible
330 heat flux is partly attributed to energy imbalance in observations, and calculated the energy balance
331 residual term: $R_{net} - (SH + LH + G)$ for summer month (June, July, and August). In wet years, GFX
332 in CLT and OGN is close to observed values; modeled latent heat flux is underestimated by ~ 10
333 W/m^2 ; modeled sensible heat flux is overestimated by $\sim 30 W/m^2$; and the residual term is ~ 17
334 W/m^2 . Hence, it is reasonable to argue that the surface energy imbalance ($\sim 17 W/m^2$) in
335 observations contributes to a large part of the $\sim 30 W/m^2$ high bias in sensible heat fluxes. In dry
336 years, the summer energy imbalance ($\sim 15 W/m^2$) is nearly equal to the high bias in sensible heat
337 flux ($\sim 15 W/m^2$).

338

339 *4.5 Impact of an organic soil horizon on annual cycle of surface energy and hydrology*

340 In the last section, it is clear that the incorporation of the top organic layer helps improve
341 the simulation of the diurnal cycle of the surface energy and hydrologic components in spring

342 season. In the following, we focus on a detailed analysis of the annual cycle of the surface energy
343 and hydrology variables for "dry" (Figure 10) versus "wet" years (Figure 11). Between June and
344 September as shown in Figure10h, the upper two soil layers were unfrozen. The topsoil is wetter
345 in OGN for both dry and wet years compared with CTL because organic soil can retain more water.
346 As discussed in section 4.2, for the deep soil layers, the liquid water content is influenced by the
347 soil temperature and the movements of the soil liquid water content between soil layers. Since the
348 soil hydraulic conductivity is higher for OGN than mineral soil, the water moves faster into deep
349 soil layers than CTL, therefore the OGN simulate higher soil liquid water content in deep layers.
350 The total soil column liquid water content keeps increasing before the soil temperature reaches
351 above the freezing point (Figure 10. g, 11.g), which is because the deep soil temperature is usually
352 higher than the top soil so ice get melts earlier in deep layer.

353 By adding an organic soil layer, the soil ice content becomes higher due to higher porosity.
354 For dry years, the impact of the organic soil on surface and sub-surface runoff is not significant
355 (Figure 10e, f). The increase in the summer latent heat flux and sensible heat flux are compensated
356 by a decrease in soil heat flux, leading to a significant decrease in summer soil temperature. In
357 winter, the latent and sensible heat fluxes are not modified by the organic soil, but increased soil
358 heat flux leads to an increased soil temperature in winter. The most prominent change by adding
359 organic soil layer is the partition between vegetation transpiration and direct ground evaporation
360 (Figure 12a and b) where the OGN simulation decreased ground surface evaporation.

361 For wet years (Figure 11), the impact of the organic soil on surface and sub-surface runoff
362 becomes more significant, especially for sub-surface runoff. The organic soil increases the surface
363 runoff during the spring snowmelt season, and increases the sub-surface runoff throughout the year.
364 Because of the higher surface layer soil ice content, the increase of subsurface flow should be due

365 to the OGN producing a wetter soil profile. The sensible heat flux also increases significantly in
366 spring, with an associated reduction in latent heat flux and soil heat flux. The summer soil
367 temperature also decreases but in a less degree than that in dry years, because the soil heat flux
368 decreases less compared with dry years. Unlike dry years, there is a significant runoff change in
369 wet years, and the ground evaporation is also decreased (Figure 12c and d). OGN produces more
370 soil-ice content and higher soil porosity, and leads to higher total soil water content than CTL
371 simulations as the higher ice content severely restricts movement of water out of the soil column.
372 In wet season, by adding an organic topsoil layer, the total column soil water increases due to the
373 infiltration of the soil water into the deep soil. This then leads to an increase in the sub-surface
374 runoff. As the consequence, the volumetric liquid water becomes higher in summer for OGN
375 compared with CTL simulation.

376

377 **5. Summary and Conclusions**

378 In this study, the Noah-MP LSM was applied at the BERMS Old Aspen site to investigate
379 the impact of incorporating a realistic organic soil horizon on simulated surface energy and water
380 cycle components. This site has an about 8-10 cm deep organic forest-floor soil horizon, typical
381 of boreal deciduous broadleaf forests.

382 When including, for the first time, an organic-soil parameterization within the Noah-MP
383 model, simulated sensible heat flux and latent heat flux are improved in spring, especially in wet
384 years, which is mostly related to the timing of spring soil thaw and warming. However, in summer
385 the model overestimated sensible heat fluxes. Such high bias in summer sensible heat flux is
386 largely attributed to surface-energy imbalance in observations, especially in dry years. Due to
387 lower thermal conductivity, the OGN simulated soil temperature was decreased during summer

388 and slightly increased during winter compared with the CTL simulation, and the OGN simulated
389 soil temperature (10-100cm) were more consistent with observations and with previous studies
390 (Lawrence and Slater 2008). Simulated top-layer soil moisture is better in OGN than in CTL in
391 summer but worse in winter.

392 Also, due to higher porosity of the organic soil, the OGN simulation was able to retain
393 more soil water content in summer. However, in winter, the OGN experiment produced less liquid
394 soil-water content due to the lower temperature and higher porosity. Since most of the soil moisture
395 is stored in soil ice, the liquid water content is reduced. However, the effects of including an
396 organic soil layer on soil temperature are not uniform throughout the soil depth and year, and those
397 effects are more prominent in summer and in deep soils.

398 For drought years, the OGN simulation substantially modified the partition between direct
399 soil evaporation and vegetation transpiration. When water is limited in drought years, the OGN
400 simulation significantly reduced the direct soil evaporation but still produced higher summer total
401 evapotranspiration. Increased latent heat flux and sensible heat flux in summer in OGN are
402 compensated by decreased soil heat flux, leading to reduced soil temperature in summer. For wet
403 years, the OGN simulated latent heat fluxes are similar to CTL except for spring season where
404 OGN produced less evaporation. In addition, the impact of the organic soil on sub-surface runoff
405 is substantial with much higher runoff throughout the season.

406 This preliminary study explored the effects of incorporating organic soil parameterization
407 in Noah-MP on the surface energy and water cycles for one flux site in a boreal forest area. Given
408 the important role of boreal forests in the regional climate system through reducing winter albedo
409 and also acting as a carbon sink and water source to the atmosphere, further work is needed to
410 evaluate the Noah-MP with organic-soil parameterization at regional scales. We plan to evaluate

411 the performance of the offline Noah-MP model and Noah-MP coupled with WRF for a broad
412 boreal forest region including Alberta and Saskatchewan.

413

414

415

416 **Acknowledgments**

417 The author Liang Chen acknowledge the support from the National Basic Research Program
418 (Grant No. 2012CB956203) and National Natural Science Foundation of China (Grant No.
419 41305062). The authors Liang Chen, Yanping Li, Alan Barr gratefully acknowledge the support
420 from Global Institute of Water Security at University of Saskatchewan. Fei Chen, Michael Barlage
421 and Bingcheng Wan appreciate the support from the Water System Program at the National Center
422 for Atmospheric Research (NCAR), and NOAA MAPP-CTB grant (NA14OAR4310186). NCAR
423 is sponsored by the National Science Foundation. Any opinions, findings, conclusions or
424 recommendations expressed in this publication are those of the authors and do not necessarily
425 reflect the views of the National Science Foundation.

426

427 **References**

- 428 Amiro BD, AG Barr, TA Black, H Iwashita, N Kljun, JH McCaughey, K Morgenstern, S
429 Murayama, Z Nesic, AL Orchansky, and N Saigusa. 2006. Carbon, energy and water fluxes at
430 mature and disturbed forest sites, Saskatchewan, Canada. *Agric. For. Meteorol.*, 136: 237-251.
- 431 Ball, J. T., I. E. Woodrow, and J. A. Berry (1987), A model predicting stomatal conductance and
432 its contribution to the control of photosynthesis under different environmental conditions, in
433 *Process in Photosynthesis Research*, vol. 1, edited by J. Biggins, pp. 221–234, Martinus Nijhoff,
434 Dordrecht, Netherlands.
- 435 Barlage, M., Tewari, M., Chen, F., Miguez-Macho, G., Yang, Z. L., and Niu, G. Y. (2015), The
436 effect of groundwater interaction in North American regional climate simulations with
437 WRF/Noah-MP, *Climatic Change*, 129(3-4), 485-498.
- 438 Bartlett, P.A., J.H. McCaughey, P.M. Lafleur and D.L. Verseghy (2002), A comparison of the
439 mosaic and aggregated canopy frameworks for representing surface heterogeneity in the
440 Canadian boreal forest using CLASS: A soil perspective, *Journal of Hydrology*, 266:15-39.
- 441 Barr, A. G., T. A. Black, E. H. Hogg, N. Kljun, K. Morgenstern, and Z. Nesic (2004), Inter-annual
442 variability in the leaf area index of a boreal aspen-hazelnut forest in relation to net ecosystem
443 production, *Agricultural and forest meteorology*, 126(3), 237–255.
- 444 Barr, A.G., K. Morgenstern, T. A. Black, J. H. McCaughey, and Z. Nesic (2006), Surface energy
445 balance closure by the eddy-covariance method above three boreal forest stands and
446 implications for the measurement of the CO₂ flux, *Agricultural and forest meteorology*, 140,
447 322-337.

448 Beringer, J., N. J. Tapper, I. McHugh, F. Chapin, A. H. Lynch, M. C. Serreze, and A. Slater (2001),
449 Impact of arctic treeline on synoptic climate, *Geophysical Research Letters*, 28(22), 4247–
450 4250.

451 Boelter, D. H. (1968), Important physical properties of peat materials. Proceedings of the 3rd
452 International Peat Congress, Quebec: 150-156.

453 Bonan, G. B. (1991), Atmosphere-biosphere exchange of carbon dioxide in boreal forests, *J.*
454 *Geophys. Res.*, 96(D4), 7301–7312, doi: 10.1029/90JD02713.

455 Bonan, G. B., D. Pollard, and S. L. Thompson. 1992. Effects of Boreal Forest Vegetation on Global
456 Climate. *Nature*, 359: 716-18.

457 Bonan, G. B. (1997), Effects of land use on the climate of the United States, *Climatic Change*, 37,
458 449–486.

459 Brutsaert, W. A. (1982), *Evaporation Into the Atmosphere*, 299 pp., D. Reidel, Dordrecht,
460 Netherlands.

461 Bryant, D., D. Nielsen, and L. Tangley (1997), *The Last Frontier Forests: Ecosystems and*
462 *Economies on the Edge*. World Resources Institute.

463 Cai, X., Z. L. Yang, C. H. David, G. Y. Niu, and M. Rodell (2014), Hydrological evaluation of the
464 Noah - MP land surface model for the Mississippi River Basin, *Journal of Geophysical*
465 *Research: Atmospheres*, 119(1), 23-38.

466 Chen, F., J. Dudhia (2001), Coupling an advanced land surface-hydrology model with the Penn
467 State-NCAR MM5 modeling system. Part I: Model implementation and sensitivity, *Monthly*
468 *Weather Review*, 129(4), 569-585.

469 Chen, F., K. Mitchell, J. Schaake, Y. Xue, H. L. Pan, V. Koren, Q. Y. Duan, M. Ek, and A. Betts
470 (1996), Modeling of land surface evaporation by four schemes and comparison with five

471 observations, *Journal of Geophysical Research: Atmospheres* (1984–2012), 101(D3), 7251–
472 7268.

473 Chen, F., M. J. Barlage, M. Tewari, R. M. Rasmussen, J. Jin, D. Lettenmaier, B. Livneh, C. Lin,
474 G. Miguez-Macho, G. Y. Niu, L. Wen, and Z. L. Yang (2014), Modeling seasonal snowpack
475 evolution in the complex terrain and forested Colorado Headwaters region: A model
476 intercomparison study, *Journal of Geophysical Research-Atmospheres*, 119, 13795-13819,
477 DOI: 10.1002/2014JD022167.

478 Chen, F. and K. Mitchell (1999), Using GEWEX/ISLSCP forcing data to simulate global soil
479 moisture fields and hydrological cycle for 1987-1988, *Journal of the Meteorological Society*
480 of Japan, 77, 1-16.

481 Chen F., G. Zhang, M. Barlage, Y. Zhang, J. A. Hicke, A. Meddens, G. Zhou, W. J. Massman, and
482 J. Frank (2015), An Observational and Modeling Study of Impacts of Bark Beetle–Caused
483 Tree Mortality on Surface Energy and Hydrological Cycles. *J. Hydrometeor*, 16, 744–761, doi:
484 <http://dx.doi.org/10.1175/JHM-D-14-0059.1>

485 Chotamonsak, C., E. P. Salathe Jr, J. Kreasuwan, and S. Chantara (2012), Evaluation of
486 precipitation simulations over Thailand using a WRF regional climate model. *Chiang Mai*
487 *Journal of Science*, 39(4), 623-638.

488 Ciais, P., P. P. Tans, M. Trolier, J. W. C. White, and R. J. Francey (1995), A large northern
489 hemisphere terrestrial CO₂ sink indicated by the ¹³C/¹²C ratio of atmospheric CO₂,
490 *SCIENCE-NEW YORK THEN WASHINGTON*, 1098-1098.

491 Clapp, R. B., and G. M. Hornberger (1978), Empirical equations for some soil hydraulic properties,
492 *Water resources research*, 14(4), 601-604.

493 Clark, M. P., et al. (2015), A unified approach for process-based hydrologic modeling: 1. Modeling
494 concept, *Water Resour. Res.*, 51, 2498–2514, doi:10.1002/2015WR017198

495 Cosgrove, B. A., D. Lohmann, K. E. Mitchell, P. R. Houser, E. F. Wood, J. C. Schaake, A. Robock,
496 C. Marshall, J. Sheffield, Q. Duan, L. Luo, R. W. Higgins, R. T. Pinker, J. D. Tarpley, and J.
497 Meng (2003), Real-time and retrospective forcing in the North American Land Data
498 Assimilation System (NLDAS) project, *J. Geophys. Res.*, 108, 8842, doi:
499 10.1029/2002JD003118, D22.

500 Dai, Y., X. Zeng, R. E. Dickinson, I. Baker, G. B. Bonan, M. G. Bosilovich, A. S. Denning, P. A.
501 Dirmeyer, P. R. Houser, G. Niu, K. W. Oleson, C. A. Schlosser, and Z. L. Yang (2003), The
502 Common Land Model. *Bull. Amer. Meteor. Soc.*, 84, 1013–1023. doi:
503 <http://dx.doi.org/10.1175/BAMS-84-8-1013>

504 Dickinson, R. E. (1986), Biosphere/atmosphere transfer scheme (bats) for the near com-
505 munity climate model, Technical report.

506 Dingman, S. L. (1994), *Physical Hydrology*, MacMillan Publishing Company, New York.

507 Ek, M. B., K. E. Mitchell, Y. Lin, E. Rogers, P. Grunmann, V. Koren, G. Gayno, and J. D. Tarpley
508 (2003), Implementation of Noah land surface model advances in the National Centers for
509 Environmental Prediction operational mesoscale Eta model, *J. Geophys. Res.*, 108, 8851,
510 doi:10.1029/2002JD003296, D22.

511 Farouki, O. T. (1981), Thermal properties of soils, Report No. Vol. 81, No. 1, CRREL Monograph

512 Gayler, S., T. Wöhling, M. Grzeschik, J. Ingwersen, H. D. Witzmann, K. Warrach-Sagi, P. Högy,
513 S. Attinger, T. Streck, and V. Wulfmeyer (2014), Incorporating dynamic root growth enhances
514 the performance of Noah-MP at two contrasting winter wheat field sites, *Water Resour. Res.*,
515 50, 1337-1356, doi:10.1002/ 2013WR014634.

516 Jordan, R. (1991), A one-dimensional temperature model for a snow cover, Spec. Rep. 91–16,
517 Cold Reg. Res. and Eng. Lab., U.S. Army Corps of Eng., Hanover, N. H.

518 Koren, V., J. C. Schaake, K. E. Mitchell, Q.-Y. Duan, F. Chen, and J. M. Baker (1999), A
519 parameterization of snowpack and frozen ground intended for NCEP weather and climate
520 models, *J. Geophys. Res.*, 104, 19,569–19,585, doi:10.1029/1999JD900232.

521 Koven, C., P. Friedlingstein, P. Ciais, D. Khvorostyanov, G. Krinner, and C. Tarnocai (2009), On
522 the formation of high-latitude soil carbon stocks: Effects of cryoturbation and insulation by
523 organic matter in a land surface model, *Geophys. Res. Lett.*, 36, L21501,
524 doi:10.1029/2009GL040150.

525 Lawrence, D. M., and A. G. Slater (2008), Incorporating organic soil into a global climate model,
526 *Climate Dynamics*, 30(2-3), 145–160.

527 Letts, M. G., N. T. Roulet, N. T. Comer, M. R. Skarupa, and D. L. Versegny (2000),
528 Parametrization of peatland hydraulic properties for the Canadian land surface scheme,
529 *Atmosphere-Ocean*, 38(1), 141–160.

530 Levine, E. R., and R. G. Knox (1997), Modeling soil temperature and snow dynamics in northern
531 forests, *J. Geophys. Res.*, 102(D24), 29407–29416, doi:10.1029/97JD01328.

532 Mölders, N., and V. E. Romanovsky (2006), Long-term evaluation of the Hydro-Thermodynamic
533 Soil-Vegetation Scheme's frozen ground/permafrost component using observations at Barrow,
534 Alaska, *J. Geophys. Res.*, 111, D04105, doi:10.1029/2005JD005957.

535 Nicolsky, D. J., V. E. Romanovsky, V. A. Alexeev, and D. M. Lawrence (2007), Improved
536 modeling of permafrost dynamics in a GCM land-surface scheme, *Geophys. Res. Lett.*, 34,
537 L08501, doi:10.1029/2007GL029525.

538 Niu, G.-Y., and Z.-L. Yang (2006), Effects of frozen soil on snowmelt runoff and soil water storage
539 at a continental scale, *J. Hydrometeorol.*, 7, 937–952, doi:10.1175/JHM538.1.

540 Niu, G.-Y., Z.-L. Yang, R. E. Dickinson, and L. E. Gulden (2005), A simple TOPMODEL-based
541 runoff parameterization (SIMTOP) for use in global climate models, *J. Geophys. Res.*, 110,
542 D21106, doi:10.1029/2005JD006111.

543 Niu, G. Y., Z. L. Yang, K. E. Mitchell, F. Chen, M. B. Ek, M. Barlage, A. Kumar, K. Manning, D.
544 Niyogi, and E. Rosero (2011), The community Noah land surface model with
545 multiparameterization options (Noah-MP): 1. Model description and evaluation with local-
546 scale measurements, *J. Geophys. Res.*, 116, D12109, doi:10.1029/2010JD015139.

547 Oleson, K. W., G. Y. Niu, Z. L. Yang, D. M. Lawrence, P. E. Thornton, P. J. Lawrence, R. Stöckli,
548 R. E. Dickinson, G. B. Bonan, S. Levis, A. Dai, and T. Qian (2008), Improvements to the
549 Community Land Model and their impact on the hydrological cycle, *J. Geophys. Res.*, 113,
550 G01021, doi: 10.1029/2007JG000563.

551 Pilotto, I. L., Rodríguez, D. A., Tomasella, J., Sampaio, G., and Chou, S. C. (2015), Comparisons
552 of the Noah-MP land surface model simulations with measurements of forest and crop sites in
553 Amazonia. *Meteorology and Atmospheric Physics*, 127(6), 711-723, doi: 10.1007/s00703-
554 015-0399-8.

555 Radforth, N. W. and Brawner, C. O. (1977). Muskeg and the northern environment in Canada. In
556 Muskeg Research Conference 1973: Edmonton, Alberta. University of Toronto Press.

557 Rinke, A., P. Kuhry, and K. Dethloff (2008), Importance of a soil organic layer for Arctic climate:
558 A sensitivity study with an Arctic RCM, *Geophys. Res. Lett.*, 35, L13709,
559 doi:10.1029/2008GL034052.

560 Thomas, G. and Rowntree, P. R. (1992), The Boreal Forests and Climate. Q.J.R. Meteorol. Soc.,
561 118, 469–497. doi: 10.1002/qj.49711850505

562 Versegny, D. L. (1991), CLASS-A Canadian land surface scheme for GCMS: I. Soil model, Int. J.
563 Climatol., 11, 111–133, doi:10.1002/joc.3370110202.

564 Viterbo, P., and A. K. Betts (1999), Impact on ECMWF forecasts of changes to the albedo of the
565 boreal forests in the presence of snow, J. Geophys. Res., 104(D22), 27803–27810,
566 doi:10.1029/1998JD200076.

567 Yang, Z. L., R. E. Dickinson, A. Henderson-Sellers, and A. J. Pitman (1995), Preliminary study
568 of spin-up processes in land surface models with the first stage data of project for
569 intercomparison of land surface parameterization schemes phase 1 (a), Journal of Geophysical
570 Research: Atmospheres, 100 (D8), 16,553–16,578.

571 Yang, Z.-L., G.-Y. Niu, K. E. Mitchell, F. Chen, M. B. Ek, M. Barlage, L. Longuevergne, K.
572 Manning, D. Niyogi, M. Tewari, and Y. Xia (2011), The community Noah land surface model
573 with multiparameterization options (Noah-MP): 2. Evaluation over global river basins, J.
574 Geophys. Res., 116, D12110, doi:10.1029/2010JD015140.

575 Zhang, G., G. Zhou, F. Chen, M. Barlage, and L. Xue (2014), A trial to improve surface heat
576 exchange simulation through sensitivity experiments over a desert steppe site, J. Hydrometeor,
577 15(2), 664–684, doi:10.1175/jhm-d-13-0113.1.

578 Zheng, D., et al. (2015), Under-canopy turbulence and root water uptake of a Tibetan meadow
579 ecosystem modeled by Noah-MP, Water Resour. Res., 51, doi:10.1002/2015WR017115

580

581
582

Table 1. Noah-MP Parameterization Options Used in this Study

Patameterizations Description	Options
Dynamic vegetation	4: table LAI, shdfac=maximum
Stomatal resistance	1: BALL-Berry (Ball et al., 1987)
Soil moisture factor for stomatal resistance	1: original Noah (Chen and Dudhia, 2001)
Runoff/soil lower boundary	2: TOPMODEL with equilibrium water table (Niu et al. 2005)
Surface layer drag Coefficient calculation	1: Monin-Obukhov (Brutsaert, 1982)
Supercooled liquid water	2: Koren's iteration (Koren et al., 1999)
Soil permeability	1: linear effects, more permeable (Niu and Yang, 2006)
Radiative transfer	3: two-stream applied to vegetated fraction
Ground surface albedo	2: CLASS (Verseghy, 1991)
Precipitation partitioning between snow and rain	1: Jordan (Jordan, 1991)
soil temp lower boundary	1: zero heat flux
snow/soil temperature time	1: semi-implicit

583

584 Table 2 Soil parameters used in Noah-MP for mineral soil texture classes (SANDY CLAY
 585 LOAM) and organic soil.

Soil Type	λ_s ($\text{W m}^{-1} \text{K}^{-1}$)	λ_{sat} ($\text{W m}^{-1} \text{K}^{-1}$)	λ_{dry} ($\text{W m}^{-1} \text{K}^{-1}$)	c_s ($\text{J m}^{-3} \text{K}^{-1} \cdot 10^6$)	θ_{sat}	κ_{sat} ($\text{m s}^{-1} \times 10^{-3}$)	Ψ_{sat} (mm)	b
Mineral	6.04	2.24	0.23	2.0	0.421	0.00445	-135	6.77
Organic	0.25	0.55	0.05	2.5	0.9	0.100	-10.3	2.7

586 The soil parameters are λ_s is the thermal conductivity of soil solids, λ_{sat} is the unfrozen saturated
 587 thermal conductivity, λ_{dry} is the dry soil thermal conductivity, c_s is the soil solid heat capacity,
 588 θ_{sat} is the saturated volumetric water content (porosity), κ_{sat} is the saturate hydraulic
 589 conductivity, Ψ_{sat} is the saturated matric potential, and b is the Clapp and Hornberger parameter.

590 **Table 3.** Averaged statistical indices for CTL and OGN simulated SH and LH compared with the
 591 observations for each year [daytime, 0800-1600 local time (LT)] (R^2 : correlation coefficient square;
 592 RMSE: root mean square error; IOA: index of agreement).

Year	SH						LH					
	CTL			OGN			CTL			OGN		
	R^2	RMSE	IOA	R^2	RMSE	IOA	R^2	RMSE	IOA	R^2	RMSE	IOA
1998	0.57	77.58	0.84	0.68	81.48	0.85	0.72	50.76	0.92	0.80	43.10	0.94
1999	0.62	62.22	0.88	0.73	69.45	0.88	0.72	46.26	0.92	0.81	37.73	0.95
2000	0.62	68.17	0.88	0.72	74.00	0.88	0.70	47.34	0.91	0.76	43.45	0.92
2001	0.74	58.82	0.91	0.80	65.40	0.91	0.79	38.55	0.94	0.85	32.84	0.96
2002	0.76	65.97	0.92	0.78	69.48	0.92	0.71	35.84	0.91	0.73	37.17	0.92
2003	0.77	55.61	0.93	0.79	56.11	0.94	0.70	37.38	0.91	0.73	41.28	0.90
2004	0.71	61.82	0.91	0.77	63.95	0.92	0.74	40.08	0.92	0.78	36.79	0.94
2005	0.64	62.84	0.89	0.79	61.24	0.92	0.69	49.36	0.91	0.82	34.61	0.95
2006	0.56	68.50	0.85	0.71	70.91	0.88	0.72	54.23	0.92	0.85	41.14	0.95
2007	0.63	64.78	0.88	0.75	66.14	0.91	0.73	51.66	0.92	0.84	38.35	0.95
2008	0.71	60.46	0.91	0.78	68.51	0.91	0.73	47.69	0.92	0.85	36.07	0.96
2009	0.70	62.83	0.90	0.76	68.13	0.91	0.76	40.79	0.93	0.81	36.57	0.95

593

594 **Figure Captions:**

595 **Figure 1.** The location of the study site (Old Aspen Flux Tower)

596 **Figure 2.** Monthly air temperature above canopy and precipitation at BERMS SK-OAS site

597 **Figure 3.** Averaged spin-up time (in years) for individual variables.

598 **Figure 4.** Observed and Noah-MP-simulated monthly soil temperature for BERMS SK-OAS site
599 at a depth of (a) top 10 cm, (b) 10-40 cm, and (c) 40-100 cm

600 **Figure 5.** Observed and Noah-MP-simulated monthly soil moisture for BERMS SK-OAS site at
601 a depth of (a) top 10 cm, (b) 10-40 cm, and (c) 40-100 cm

602 **Figure 6.** Observed and the Noah-MP simulated (CTL and OGN) monthly sensible and latent heat
603 flux above canopy

604 **Figure 7.** Scatterplots of the monthly-averaged (a) sensible, (b) latent heat fluxes (W m^{-2}) for
605 CTL versus the observation above canopy; the monthly-averaged (c) sensible, (d) latent heat fluxes
606 (W m^{-2}) for OGN versus the observation above canopy. The color represents each month from
607 January (1) to December (12).

608 **Figure 8.** Comparison of the seasonal averaged diurnal cycle of the sensible and latent heat fluxes
609 at OAS site for drought years

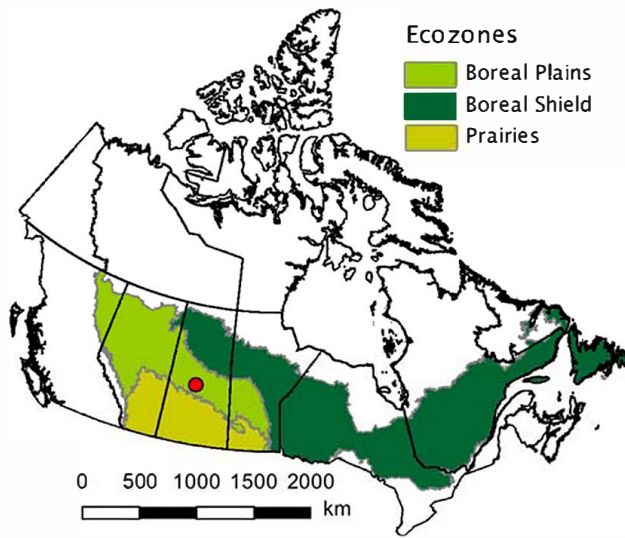
610 **Figure 9.** Comparison of the seasonal averaged diurnal cycle of the sensible and latent heat fluxes
611 at OAS site for wet years

612 **Figure 10.** Annual cycle of selected surface energy and hydrologic cycle fields for drought years.
613 Black line is the observation. Black line is the observation. Note that (a) is the observed
614 precipitation, (b) is sensible heat flux, (c) is latent heat flux, (d) is ground heat flux, (e) is surface
615 runoff, (f) is underground runoff, (g) is the total column soil liquid water content changes, (h) is
616 the total column soil ice water content changes.

617 **Figure 11.** Annual cycle of selected surface energy and hydrologic cycle fields for wet years.
618 Black line is the observation. Note that (a) is the observed precipitation, (b) is sensible heat flux,
619 (c) is latent heat flux, (d) is ground heat flux, (e) is surface runoff, (f) is underground runoff, (g) is
620 the total column soil liquid water content changes, (h) is the total column soil ice water content
621 changes.

622 **Figure 12.** Water budgets: blue lines are accumulated surface runoff (mm), blue dots are
623 accumulated underground runoff (mm), red lines are accumulated evaporation of intercepted water
624 (mm), red dots are accumulated ground surface evaporation (mm), red dash lines are accumulated
625 transpiration (mm), green lines are snow water equivalent changes (mm), purple lines are soil
626 water content changes in the soil column (mm), (a) and (b) are averaged for 2002–2003, (c) and
627 (d) are averaged for 2005-2006.

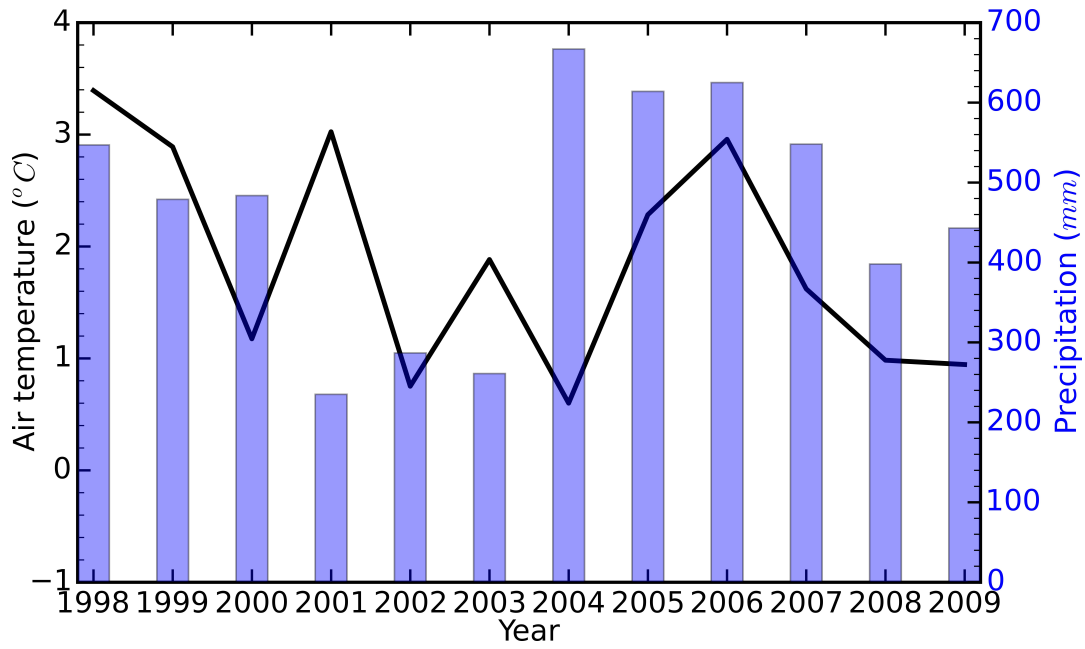
628



629

630 **Figure 1.** The location of the study site (Old Aspen Flux Tower)

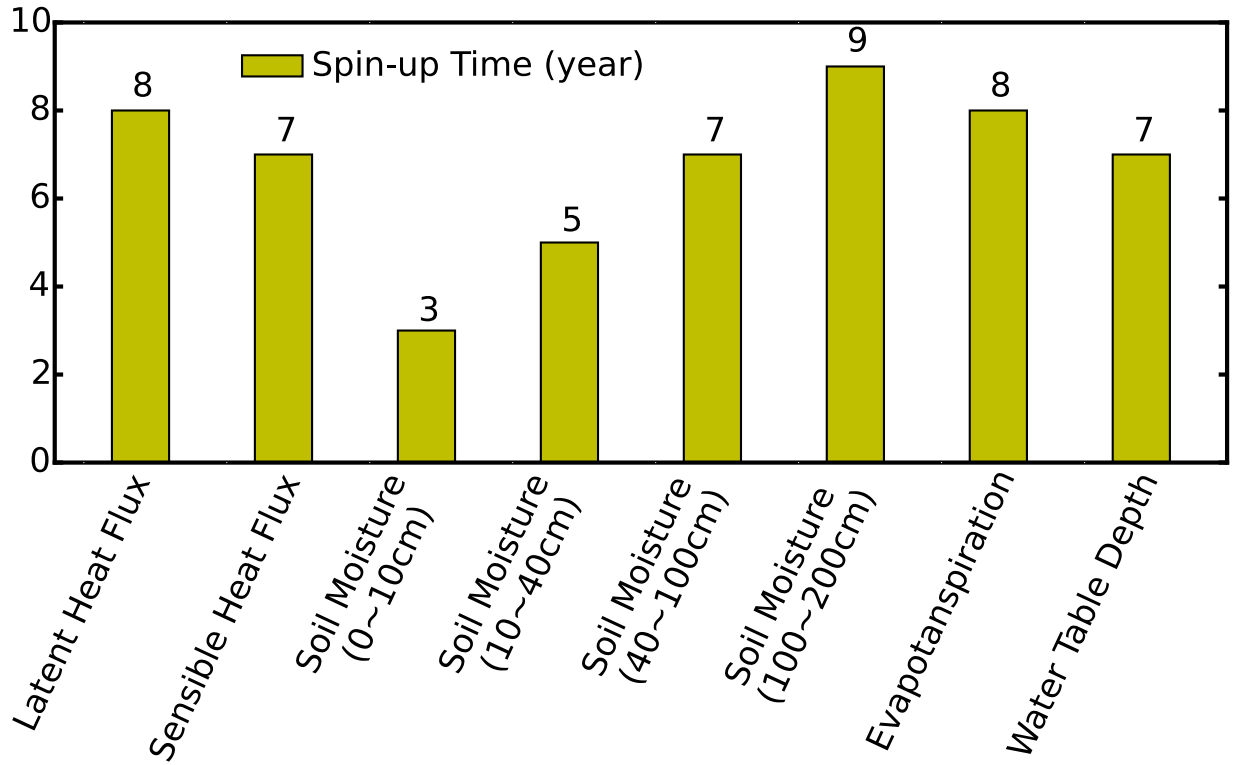
631



632

633 **Figure 2.** Monthly air temperature above canopy and precipitation at BERMS SK-OAS site

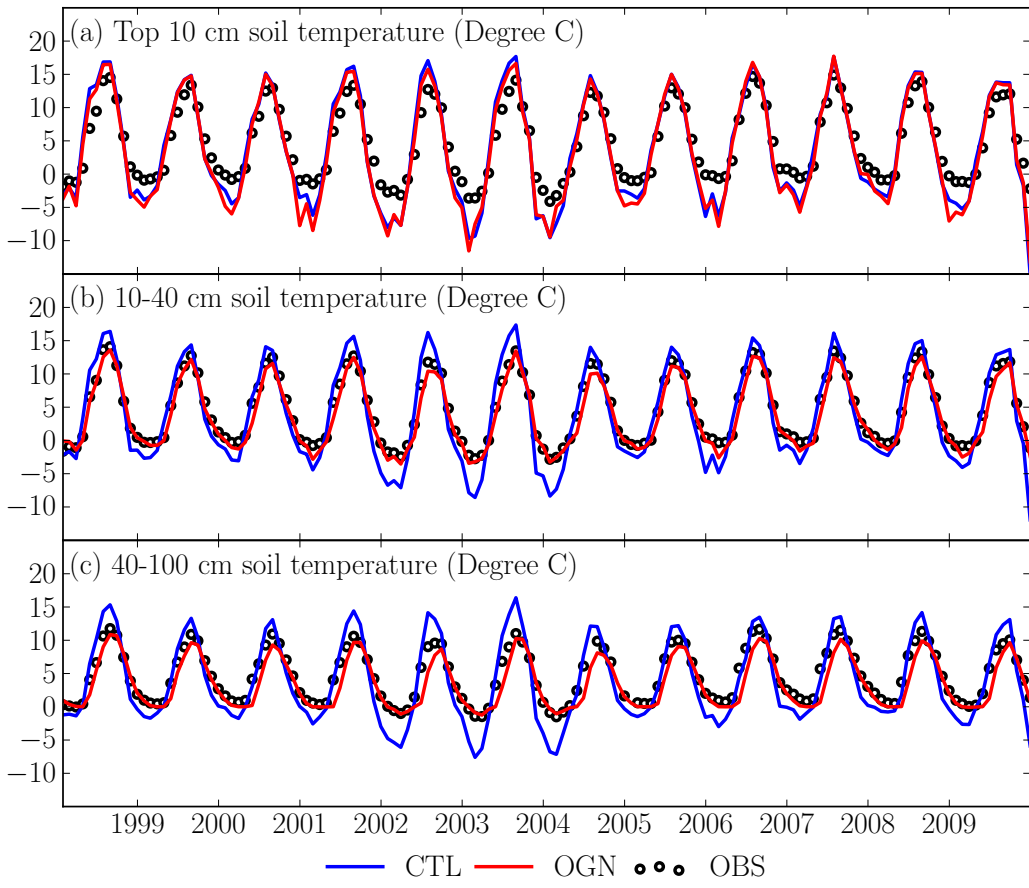
634



635

636 **Figure 3.** Averaged spin-up time (in years) for individual variables.

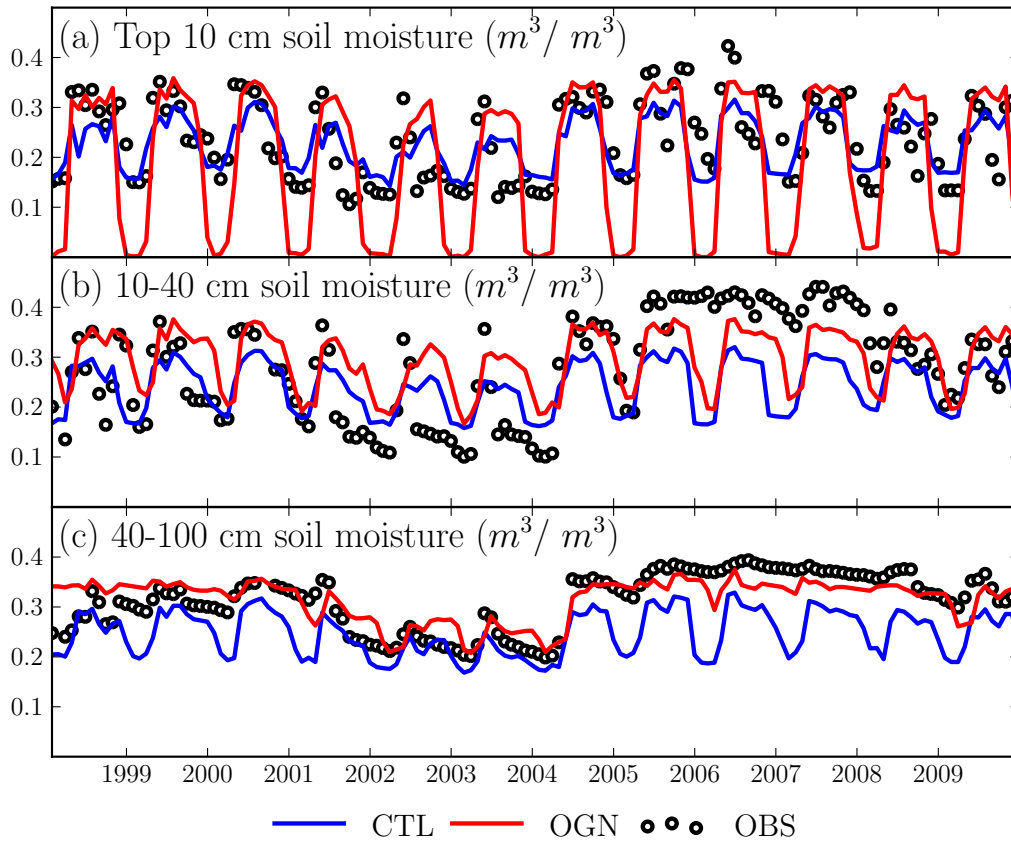
637



638

639 **Figure 4.** Observed and Noah-MP-simulated monthly soil temperature for BERMS SK-OAS site
 640 at a depth of (a) top 10 cm, (b) 10-40 cm, and (c) 40-100 cm

641

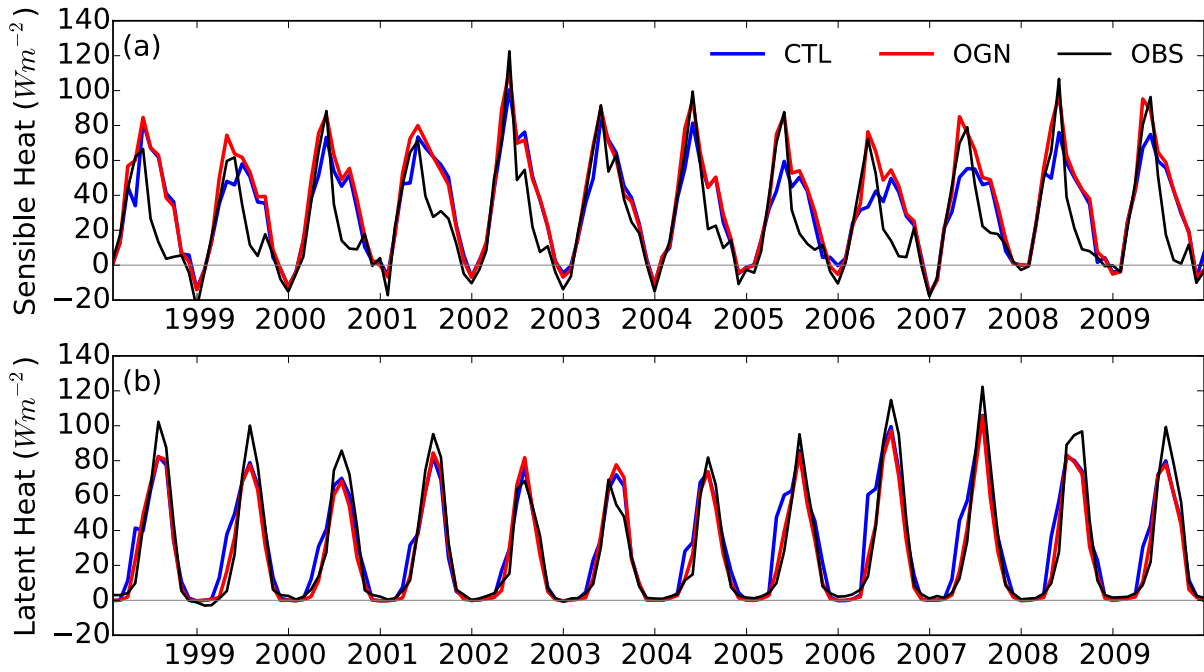


642

643 **Figure 5.** Observed and Noah-MP-simulated monthly soil moisture for BERMS SK-OAS site at

644 a depth of (a) top 10 cm, (b) 10-40 cm, and (c) 40-100 cm

645

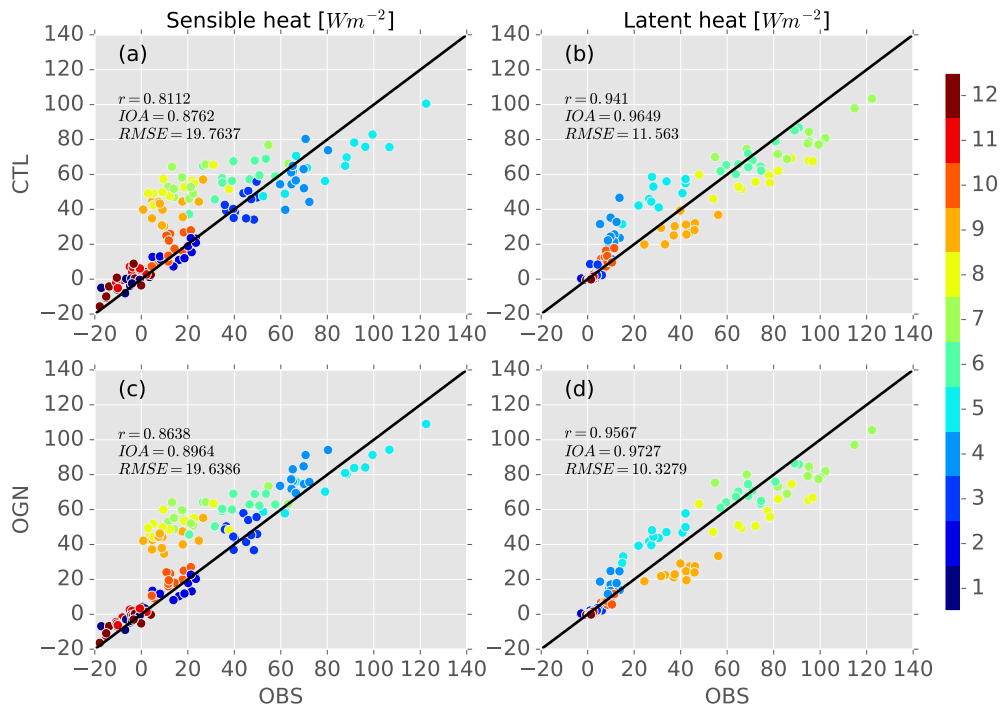


646

647 **Figure 6.** Observed and the Noah-MP simulated (CTL and OGN) monthly sensible and latent heat

648 flux above canopy

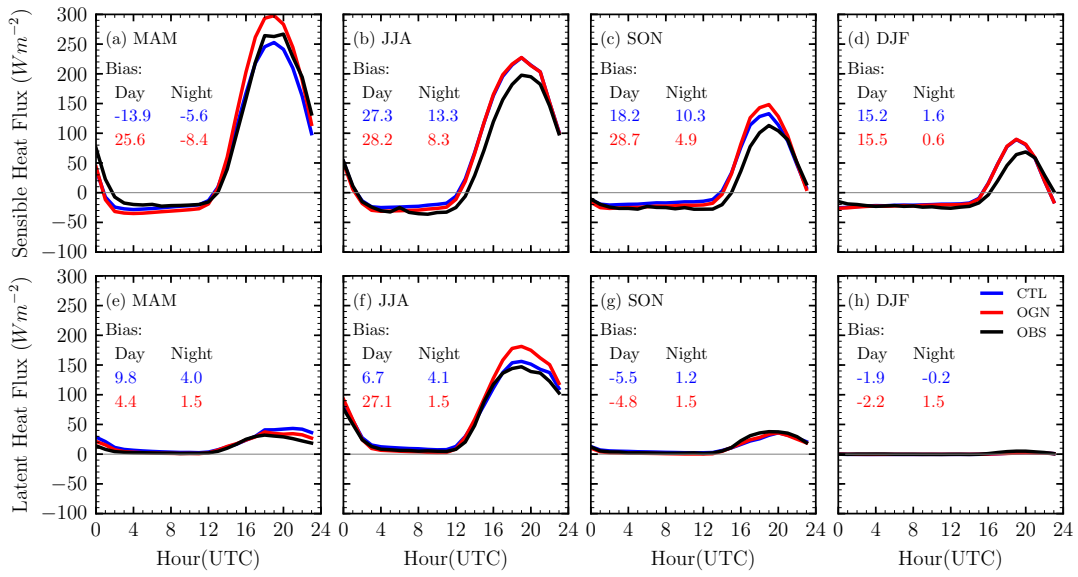
649



650

651 **Figure 7.** Scatterplots of the monthly-averaged (a) sensible, (b) latent heat fluxes ($W m^{-2}$) for
 652 CTL versus the observation above canopy; the monthly-averaged (c) sensible, (d) latent heat fluxes
 653 ($W m^{-2}$) for OGN versus the observation above canopy. The color represents each month from
 654 January (1) to December (12).

655

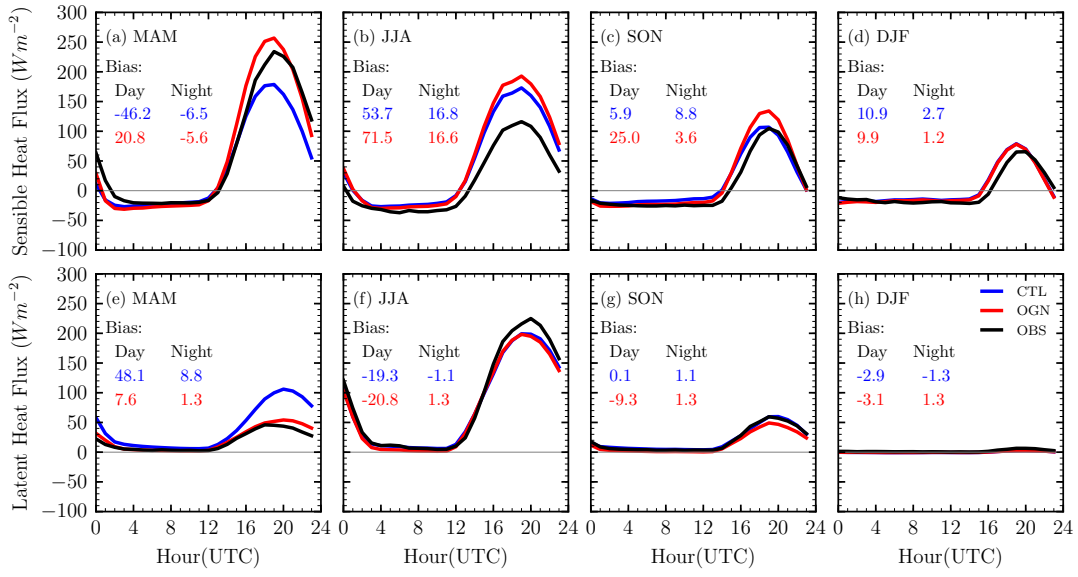


656

657 **Figure 8.** Comparison of the seasonal averaged diurnal cycle of the sensible and latent heat fluxes

658 at OAS site for drought years

659

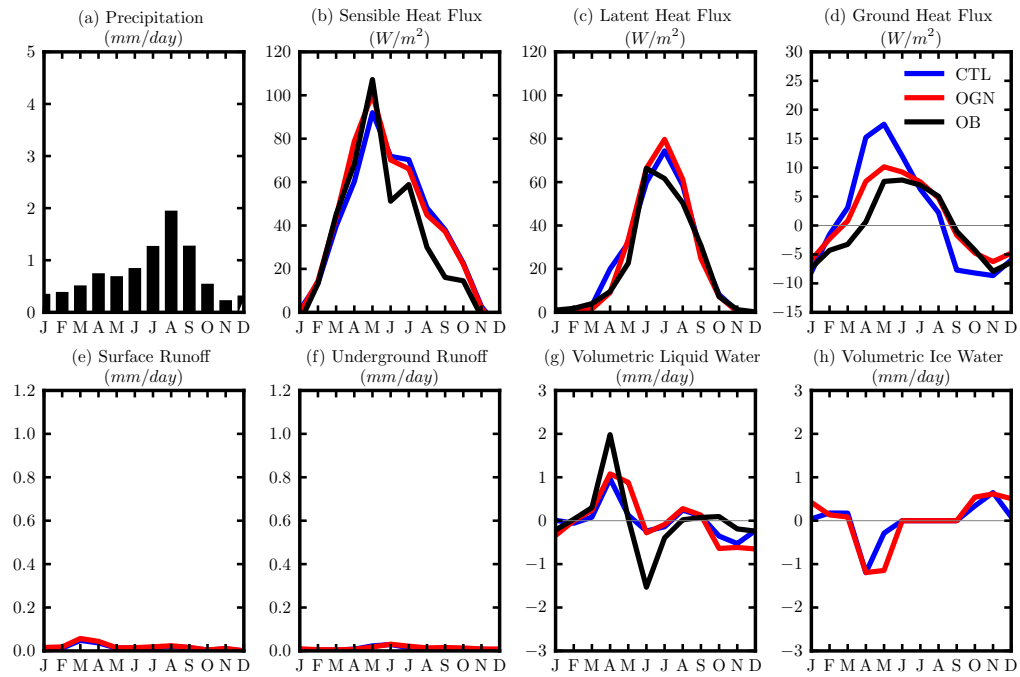


660

661 **Figure 9.** Comparison of the seasonal averaged diurnal cycle of the sensible and latent heat fluxes

662 at OAS site for wet years

663



664

665 **Figure 10.** Annual cycle of selected surface energy and hydrologic cycle fields for drought years.

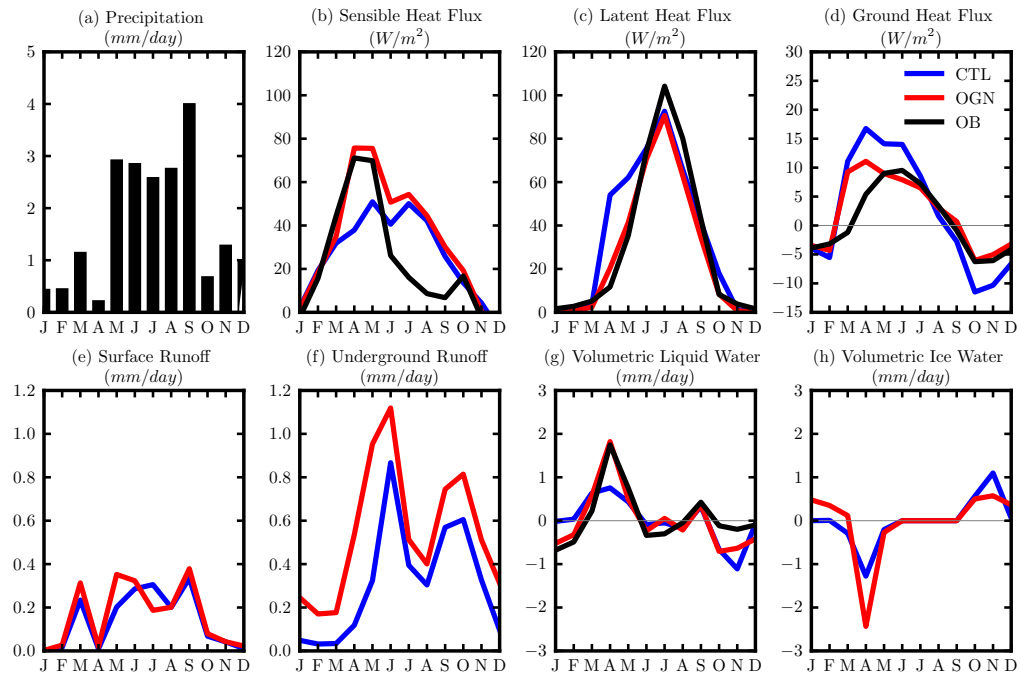
666 Black line is the observation. Black line is the observation. Note that (a) is the observed

667 precipitation, (b) is sensible heat flux, (c) is latent heat flux, (d) is ground heat flux, (e) is surface

668 runoff, (f) is underground runoff, (g) is the total column soil liquid water content changes, (h) is

669 the total column soil ice water content changes.

670



671

672 **Figure 11.** Annual cycle of selected surface energy and hydrologic cycle fields for wet years.

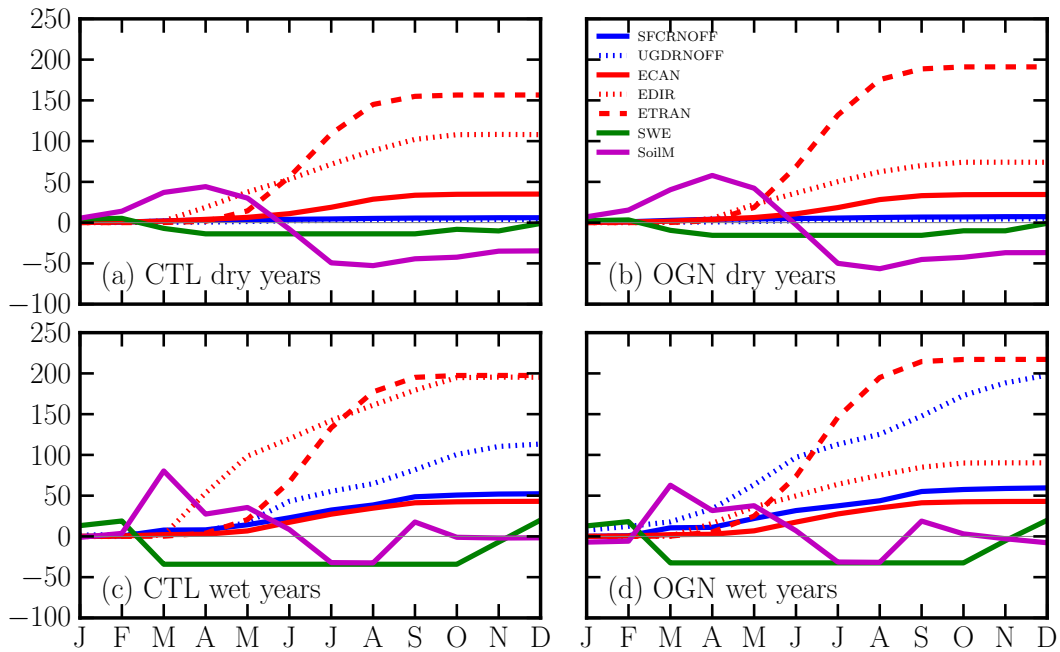
673 Black line is the observation. Note that (a) is the observed precipitation, (b) is sensible heat flux,

674 (c) is latent heat flux, (d) is ground heat flux, (e) is surface runoff, (f) is underground runoff, (g) is

675 the total column soil liquid water content changes, (h) is the total column soil ice water content

676 changes.

677



678

679 **Figure 12.** Water budgets: blue lines are accumulated surface runoff (mm), blue dots are
 680 accumulated underground runoff (mm), red lines are accumulated evaporation of intercepted water
 681 (mm), red dots are accumulated ground surface evaporation (mm), red dash lines are accumulated
 682 transpiration (mm), green lines are snow water equivalent changes (mm), purple lines are soil
 683 water content changes in the soil column (mm), (a) and (b) are averaged for 2002–2003, (c) and
 684 (d) are averaged for 2005-2006.